

Article

A Highly Selective and Sensitive Sequential Recognition Probe Zn^{2+} and $H_2PO_4^-$ Based on Chiral Thiourea Schiff Base

Shan Yang ^{1,†}, Yichuan Huang ^{1,†}, Aidang Lu ^{1,*} , Ziwen Wang ^{2,*}  and Hongyan Li ^{1,*}

¹ School of Chemical Engineering and Technology, Hebei University of Technology, Tianjin 300401, China; 17865513875@163.com (S.Y.); yichuan1026@163.com (Y.H.)

² Tianjin Key Laboratory of Structure and Performance for Functional Molecules, College of Chemistry, Tianjin Normal University, Tianjin 300387, China

* Correspondence: luaidang@hebut.edu.cn (A.L.); hxywz@tjnu.edu.cn (Z.W.); hyl@hebut.edu.cn (H.L.)

† These authors contributed equally to this work.

Abstract: A series of novel chiral thiourea fluorescent probes **HL**₁–**HL**₆ were designed and synthesized from (1*R*,2*R*)-1,2-diphenylethylenediamine, phenyl isothiocyanate, and different substituted salicylic aldehydes. All of the compounds were confirmed by ¹H NMR, ¹³C NMR, and HRMS. They exhibit high selectivity and sensitivity to Zn^{2+} in the presence of nitrate ions with the detection limit of 2.3×10^{-8} M (**HL**₅). Meanwhile, their zinc (II) complexes (**L**- $ZnNO_3$) showed continuous response to $H_2PO_4^-$ in acetonitrile solution. The identification processes could further be verified by supramolecular chemistry data analysis, X-ray single-crystal diffraction analysis, and theoretical study. The research provides reliable evidence for an explanation of the mechanism of action of thiourea involved in coordination, which is important for the application of thiourea fluorescent probes. In short, the sensors **HL**₁–**HL**₆ based on chiral thiourea Schiff base will be promising detection devices for Zn^{2+} and $H_2PO_4^-$.

Keywords: chiral thiourea; Schiff base; fluoresce; Zn^{2+} detection; $H_2PO_4^-$ detection



Citation: Yang, S.; Huang, Y.; Lu, A.; Wang, Z.; Li, H. A Highly Selective and Sensitive Sequential Recognition Probe Zn^{2+} and $H_2PO_4^-$ Based on Chiral Thiourea Schiff Base. *Molecules* **2023**, *28*, 4166. <https://doi.org/10.3390/molecules28104166>

Academic Editors: Renhua Qiu, Lifeng Peng and Longzhi Zhu

Received: 5 May 2023

Revised: 15 May 2023

Accepted: 16 May 2023

Published: 18 May 2023



Copyright: © 2023 by the authors. Licensee MDPI, Basel, Switzerland. This article is an open access article distributed under the terms and conditions of the Creative Commons Attribution (CC BY) license (<https://creativecommons.org/licenses/by/4.0/>).

1. Introduction

In recent years, widespread research has been undertaken on the detection of metal ions [1–5] and inorganic anions [6–9], particularly within the development of selective ion probes, which has more generally become a popular topic in scientific research. Zn^{2+} is the second most common element in the human body, after iron, and not only plays an important role in protein structure, catalysis, transcription, and regulation, but is also closely associated with nerve signal transmission, enzyme regulation, and gene expression [10]. Excessive concentrations of Zn^{2+} can cause neurodegenerative diseases such as Alzheimer's disease and Parkinson's disease [11–14]. Therefore, the development of methods to accurately determine trace amounts of Zn^{2+} and for its removal prior to entering the body are important research goals.

Among the various anions, the detection of phosphates most commonly the subject of research. Phosphates are the key substrates of many biochemical reactions and the main components of biomolecules [15–18]. Phosphate and its derivatives are important nutrients, and the basic life activities of organisms are closely related to phosphate. Phosphate is not only a component of some important structures of plants but is also a catalyst for many key biochemical reactions in plants, which can promote the development of plant roots and the early growth of seedlings. The life activities of organisms are also closely related to phosphates [18]. Phosphates can regulate the level of 1,25-(OH)₂-vitamin D in human plasma [19] and react with hydroxyl groups to form phosphate esters, thus allowing monomers to polymerize into relatively stable long chain skeletons (DNA and RNA skeletons) [20]. In addition, phosphate is also involved in ATP energy supply, ion channel regulation, enzymatic reactions, and intercellular signal transduction [8]. Unfortunately, a

large amount of phosphate deposition can lead to a lack of dissolved oxygen in water and algae eutrophication [18].

At present, there are many conventional methods to detect Zn^{2+} ions including ion chromatography, atomic absorption spectrometry, and ion exchange [21]. Among these methods, chemical sensors are widely used to detect many biological and environmental heavy metal pollutants because of their advantages such as higher sensitivity, lower cost, and faster detection [22,23]. In particular, the multi-functional sensors used for the sequential recognition of cations and anions have remarkable advantages in special applications for their low cost, quick response, and convenient operation. Most of the currently available fluorescent probes can only analyze certain types of anions or cations, and there are few fluorescent sensors with the sequential recognition of Zn^{2+} and $H_2PO_4^-$ [24,25].

In this work, a series of chiral thiourea Schiff base fluorescent probes (**HL**₁–**HL**₆) were designed and synthesized starting from (1*R*,2*R*)-1,2-diphenylethylenediamine, phenyl isothiocyanate, and different substituted salicylic aldehydes (Figure 1). They were explored for the first time for fluorescent-responsive Zn^{2+} detection in the presence of nitrate ions in acetonitrile. Meanwhile, their zinc (II) complexes (**HL**- Zn^{2+} - NO_3^-) showed continuous response to $H_2PO_4^-$ in acetonitrile solution. Up to now, the detection mechanisms of thiourea probes have been reported mostly by 1H NMR titration or Job's plot titration experiments to speculate the possible coordination mode, and some of the assays do not provide practical and reliable data [26,27]. Here, we successfully elucidated the mechanism of metal ion recognition by this kind of thiourea Schiff base fluorescent probe using supramolecular chemistry data analysis, X-ray single-crystal diffraction analysis, and theoretical study. The research provides reliable evidence for an explanation of the mechanism of action of thiourea involved in coordination, which is important for the application of thiourea fluorescent probes. The probes in our work have the advantages of high sensitivity and low detection limits. In short, the sensors **HL**₁–**HL**₆ based on chiral thiourea Schiff base will be promising detection devices for Zn^{2+} and $H_2PO_4^-$.

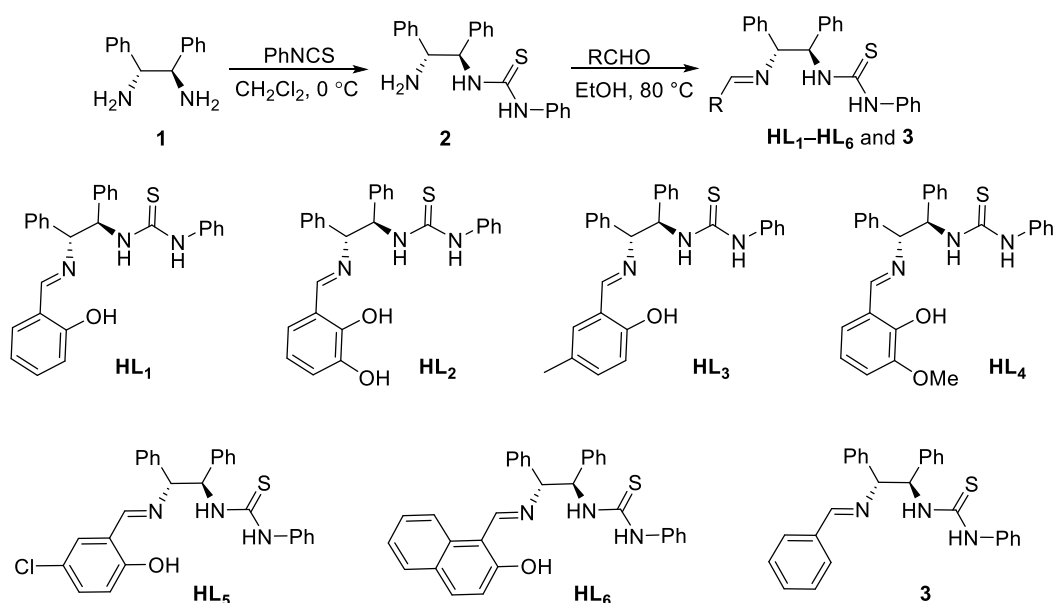


Figure 1. Synthesis of **HL**₁–**HL**₆ and compound **3**.

2. Results and Discussion

2.1. Fluorescence Spectroscopic Studies of **HL**₁–**HL**₆ and **3** in the Presence of Metal Ions

2.1.1. Cation Selectivity Experiments

Selectivity experiments were carried out for **HL**₁–**HL**₆ and **3** by examining the emission spectra in the presence of different metal ions (Ag^+ , Na^+ , K^+ , Co^{2+} , Fe^{3+} , Cu^{2+} , Cd^{2+} , Cr^{3+} ,

Mg²⁺, Pb²⁺, Ni²⁺, Zn²⁺, Fe²⁺, Hg²⁺, Ca²⁺) in filtered Milli-Q water. As shown in Figure 2a, HL₁ displayed a weak emission peak at 447 nm in acetonitrile solution when excited at 380 nm. Upon the addition of various metal ions in HL₁, the emission spectrum was only significantly enhanced with Zn²⁺, whereas Cd²⁺ and Pb²⁺ caused a very small enhancement in the emission intensity at wavelengths corresponding to 400 and 600 nm, respectively. This observation demonstrates the high selectivity of HL₁ towards Zn²⁺ compared to other metal ions, including Cd²⁺ and Pb²⁺. Molecular probes that show turn-on fluorescence signaling upon interaction with Zn²⁺ also often interact with Cd²⁺/Pb²⁺, resulting in turn-on signaling [28]. In contrast, blue fluorescence was observed in the probe solution upon interaction with Zn²⁺ under a 365 nm UV lamp (Figure 2a, inset). In the case of other metal cations, the fluorescence spectra almost remained unchanged (Figure 2a). Subsequently, the selectivity of the HL₁–HL₆ and 3 probes for various metal ions was investigated (Figures S1 and S2). The addition of Zn²⁺ resulted in a prominent luminescence enhancement (Figures S1 and S2), whereas the addition of a large excess of other competitive cations caused only slight luminescent changes (Figure S2), with the exception of 3 (Figures S1f and S2g). The fluorescence emission produced by the interaction between HL₅ and Zn²⁺ was the strongest, whereas that with HL₂ was the weakest. The strength of the other observed emissions was at a medium level, except for compound 3. The difference in the fluorescence intensity of other compounds mainly depends on the difference in the side substituents of salicylaldehyde. The fluorescence intensity of HL₅ is better than that of HL₃, and obviously stronger than that of HL₄, HL₆, and HL₂. When salicylaldehyde contains electron-donating groups, such as –OH, –CH₃, and –OCH₃, it can be increased the density of the electron cloud on the benzene ring, resulting in the weakening of the coordination ability of HL with zinc ions. Under the combined influence of the inductive effect and mesomeric effect, HL₅ containing –Cl has the strongest coordination ability with Zn²⁺. Compound 3 without the –OH in the benzene ring structure of the benzylidene group was not able to recognize Zn²⁺, which demonstrates that the phenolic hydroxyl group was involved in the formation of complexes. HL₁–HL₆ probes showed high selectivity in sensing Zn²⁺ and can be used as “turn-on” luminescent molecular probes toward Zn²⁺.

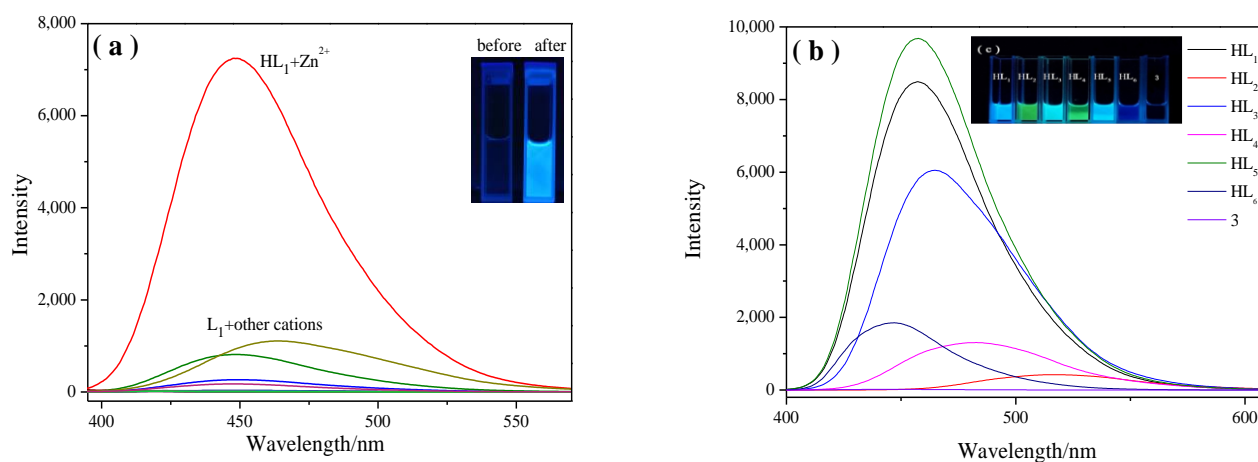


Figure 2. (a) Change in the emission spectra of HL₁ upon the addition of different metal ions in acetonitrile. Inset: Visual color change of HL₁ before and after the addition of Zn²⁺ under a 365 nm UV lamp; (b) fluorescence spectra of HL₁–HL₆ and compound 3 after the addition of Zn²⁺; (c) color of HL₁–HL₆ and compound 3 solution with the addition of Zn²⁺ under a UV lamp.

2.1.2. Cation-Competitive Experiments

The competitive experiments between the HL₁–HL₆ probes and coexisting metal ions were investigated on the basis of emission spectra. As shown in Figure 3a, whether in the absence or presence of competitive metal ions, the strong increase in the emission intensity of the HL₁ probe was observed upon the addition of Zn²⁺. Although Cd²⁺ and Pb²⁺, among

the verified cations, triggered enhancements in emission, these were negligible compared to that of Zn^{2+} . When HL_2 – HL_6 were treated with 10 equiv. of other metal ions and 2 equiv. of Zn^{2+} , similar luminescence changes were also observed. The effect was almost the same as that resulting from the addition of Zn^{2+} (Figure S3). In all, the coexistence of these cations had a negligible effect on the detection of Zn^{2+} in the tested media.

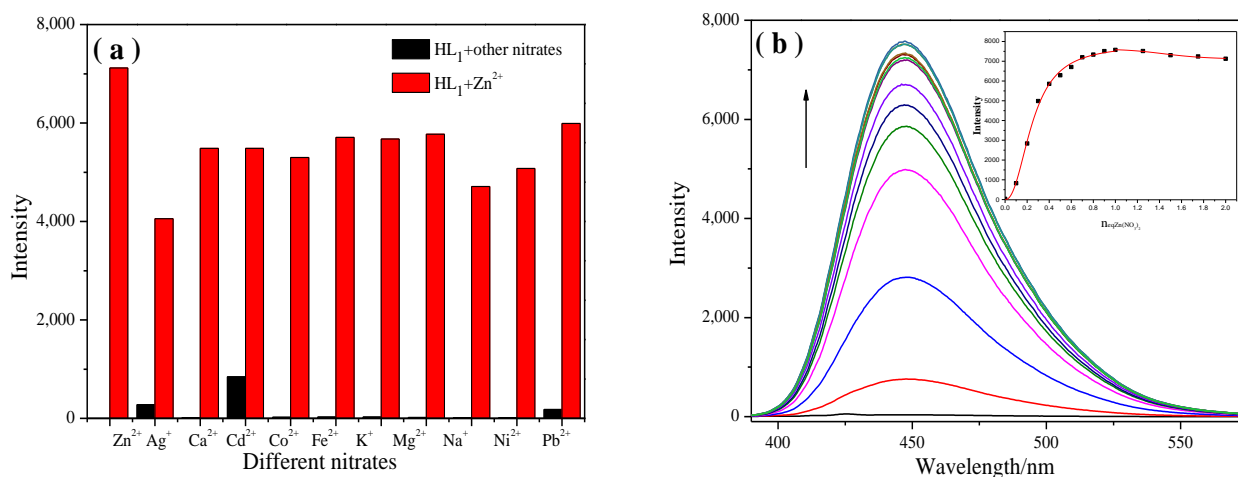


Figure 3. (a) Fluorescence intensities of HL_1 excited at 377 nm upon the addition of $\text{Zn}(\text{NO}_3)_2$ in the presence of nitrates subject to interference. The black bars represent the emission intensities of HL_1 in the presence of nitrates of interest (10.0 equiv.). The red bars represent the change in emission upon the subsequent addition of $\text{Zn}(\text{NO}_3)_2$ (2.0 equiv.) to the above solution; (b) emission spectra of HL_1 in acetonitrile solution in the presence of an increasing amount of Zn^{2+} in filtered Milli-Q water. Inset: Fluorescence intensity of HL_1 depending on the Zn^{2+} in the range from 0 to 2.0 equiv.

2.1.3. Study of the Reversibility and Dependence of Fluorescence on Solvent, pH, Different Zinc Salts

To examine whether the complexation of HL and Zn^{2+} is reversible, we added an aqueous solution of Na_2EDTA during detection. Upon the addition of Na_2EDTA (1.0 equiv.) to the solution of HL_1 containing Zn^{2+} , the emission intensity of the mixture solution decreased significantly with the luminescence quenching. It seems logical that the fluorescent intensity observed in Figure 4a is inversely proportional to the stability of the complex formed by L-Zn with the anions as the fluorescence of the complex can be quenched by Na_2EDTA [29]. Changes in the solvent and pH had non-negligible effects on the detection effect of the fluorescent probe. Therefore, we investigated the dependence of the fluorescence emission intensity on solvent and pH during the recognition of Zn^{2+} by HL_1 . Interestingly, the intensity of the fluorescence emission spectrum in the acetonitrile solvent was significantly enhanced, and $\text{CH}_3\text{CH}_2\text{OH}$ was also a good choice under some conditions (Figure 4b). Further investigation of the effect of pH on the detection of Zn^{2+} was carried out by adjusting the required pH using 0.01 M HCl or 0.01 M NaOH . The fluorescence emission intensity was stable within the pH range of 5.5–9.0, which includes physiological range basically (Figure 4c). Under strong acid or base conditions, the stability of the $\text{C}=\text{N}$ bond and the presence of $-\text{OH}$ can have a significant impact, resulting in fluorescence quenching. To judge whether the probe can selectively recognize Zn^{2+} in different zinc salts, an examination of the sensitivity of the L_1 probe to several different zinc salts (zinc chloride, zinc gluconate, and zinc nitrate) was undertaken using fluorescence spectroscopy. However, the fluorescence spectrum enhancement of the L_1 probe was not obvious when it was complexed with zinc chloride and zinc gluconate, and the fluorescence enhancement phenomenon only appeared when it interacted with zinc nitrate (Figure 4d). Therefore, we preliminarily speculate that the HL probe recognizes Zn^{2+} in the presence of NO_3^- , which is involved in the coordination process.

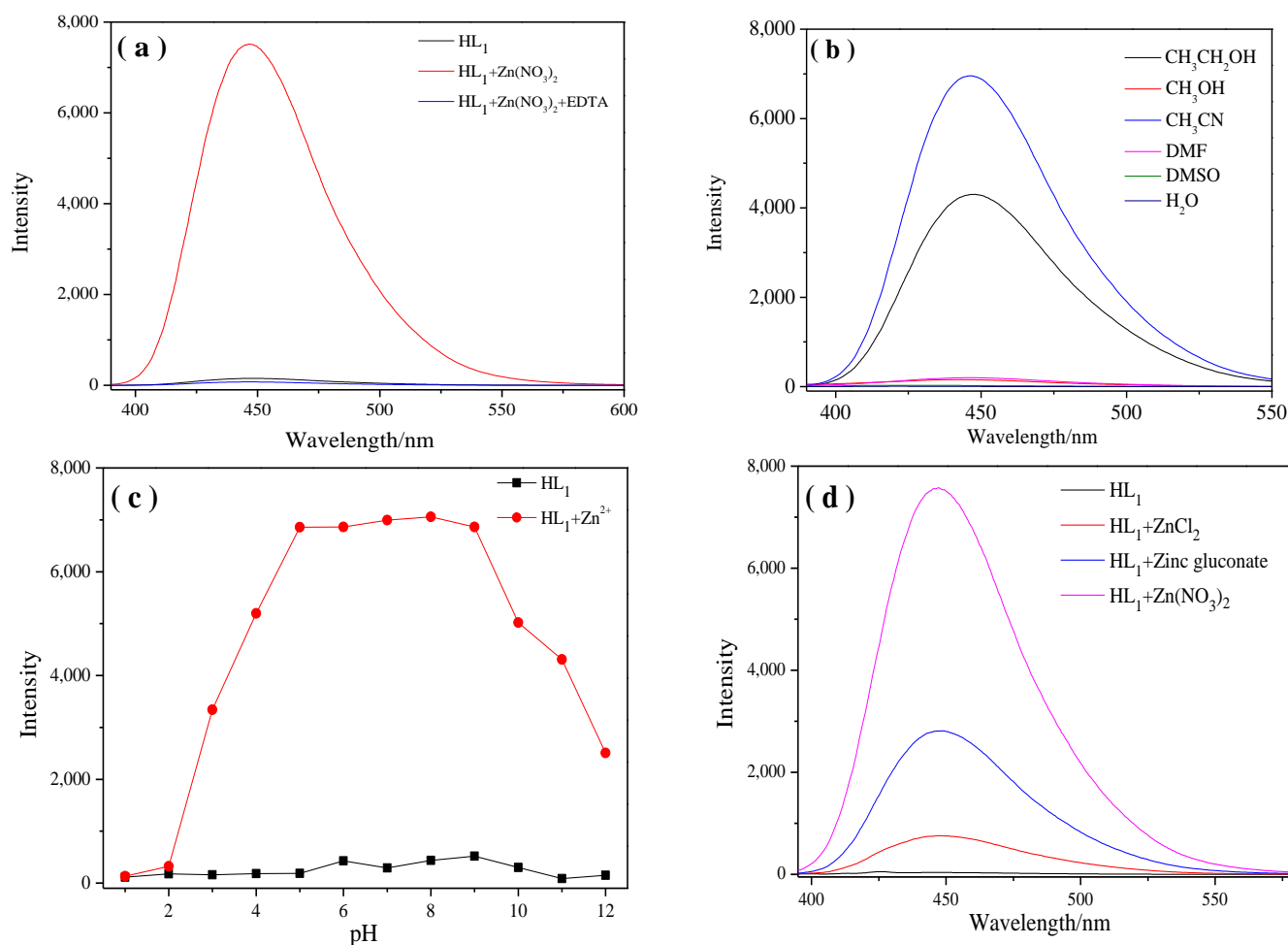


Figure 4. (a) Zn²⁺ and EDTA were added to a solution of HL₁ in acetonitrile; (b) emission spectra of the HL₁ probe in different solvents, excitation at 380 nm; (c) fluorescence spectra of HL₁ interacting with Zn²⁺ at different pH in acetonitrile; (d) effects on fluorescence spectra of HL₁ using different zinc salts in acetonitrile.

2.1.4. Zn²⁺ Titration Analysis

Fluorescence titration spectra were examined to obtain additional information regarding the binding form of the HL₁ probe with Zn²⁺ (Figure 3b). After adding Zn²⁺ to the solution, HL₁ exhibited a broad emission profile peaking at 447 nm in acetonitrile solution and displayed a linear enhancement in the emission intensity. The increase in the intensity of the emission spectra stopped after the addition of 1 equivalent of metal ions, which suggested 1:1 binding stoichiometry between HL₁ and Zn²⁺ (Figure 3b, inset). In addition, the photoluminescence titration experiments of individual complexes of HL₂–HL₆ with Zn²⁺ in varying concentrations were carried out by monitoring the emission intensity changes. Similarly, the emission intensity of HL₂–HL₆ increased continuously until the addition of 1 equiv. of Zn²⁺; the further addition of Zn²⁺ induced only minor changes in the luminescence spectra (Figure S4).

2.2. Binding Mechanism

According to literature reports [30–32], the supramolecular chemical data analysis method was adopted to analyze the combination of host and guest, and the binding constants of host and guest 1:1, 1:2, and 2:1 were simulated, respectively. The results are shown in Table 1. The detection limit of HL₁ for Zn²⁺ was calculated as $3\sigma/k$, where σ is the standard deviation of the blank measurement and k is the slope of the plot of the emission intensity ratio versus Zn²⁺ concentration [33]. The limit of detection (LOD) of HL₂–HL₆

for Zn^{2+} are 2.8×10^{-8} M, 2.2×10^{-6} M, 3.3×10^{-8} M, 1.4×10^{-7} M, 2.3×10^{-8} M, and 1.74×10^{-7} M, respectively. The fluorescence intensity of the **HL** probe had a good linear relationship with the concentration of $\text{Zn}(\text{NO}_3)_2$ and had a lower detection limit, which could be used for the quantitative detection of $\text{Zn}(\text{NO}_3)_2$.

Table 1. Job plot shapes of **HL**₁ at various concentrations and $K^{1:1}$, $K^{1:2}$ to $K^{2:1}$ ratios. $K^{1:1} = 1000$, $K^{1:2} = 100$, $K^{2:1} = 100$ were assumed.

Parameter (Bounds)	Optimized	Error	Initial
K ($0 \rightarrow \infty$)	8607.30 M^{-1}	$\pm 9.1006\%$	100.00 M^{-1}
K_{11} ($0 \rightarrow \infty$)	3376.76 M^{-1}	$\pm 5.2092\%$	1000.00 M^{-1}
K_{12} ($0 \rightarrow \infty$)	4790.08 M^{-1}	$\pm 26.9494\%$	100.00 M^{-1}
K_{11} ($0 \rightarrow \infty$)	3576.53 M^{-1}	$\pm 9.1090\%$	1000.00 M^{-1}
K_{21} ($0 \rightarrow \infty$)	$-277,004.73 \text{ M}^{-1}$	$\pm -4.6365\%$	100.00 M^{-1}

To further confirm the coordination mechanism of ligand **HL** with zinc nitrate, the crystals were obtained and analyzed. Single crystals of **HL**₄ (CCDC: 2077389) and **L**₄- ZnNO_3 (CCDC: 2077390) suitable for X-ray diffraction study were obtained by the slow evaporation of mixed solutions of acetonitrile/methanol at room temperature. **L**₄- ZnNO_3 was cultured in proportions of equal amounts and an excessive amount of $\text{Zn}(\text{NO}_3)_2$, and the complex single crystal with a coordination mode of 1:1 was obtained. The ellipsoid diagrams of **HL**₄ and **L**₄- ZnNO_3 shown in Figure 5 were obtained by X-ray single crystal diffraction analysis. The corresponding crystallographic data are summarized in Table S1, and selected bond lengths and angles are listed in Table S2. The single crystal of the complex **L**₄- ZnNO_3 clearly showed the formation of a six-membered ring and a seven-membered ring. The central Zn atom adopted a four-coordination method, which was, respectively, connected to the S atom ($\text{Zn-S} = 2.314(16) \text{ \AA}$), the N atom of $\text{C}=\text{N}$ ($\text{Zn-N3} = 2.020(5) \text{ \AA}$), the O atom of the salicylaldehyde phenolic hydroxyl group ($\text{Zn-O1} = 1.946(5) \text{ \AA}$), and the O atom of NO_3 ($\text{Zn-O3} = 2.043(5) \text{ \AA}$). This coordination mode is consistent with the coordination mode of monodentate ligands reported in the literature [34–36]. The crystal structure indicates that the N atom on the thiourea group was not coordinated, and that only the S atom is involved.

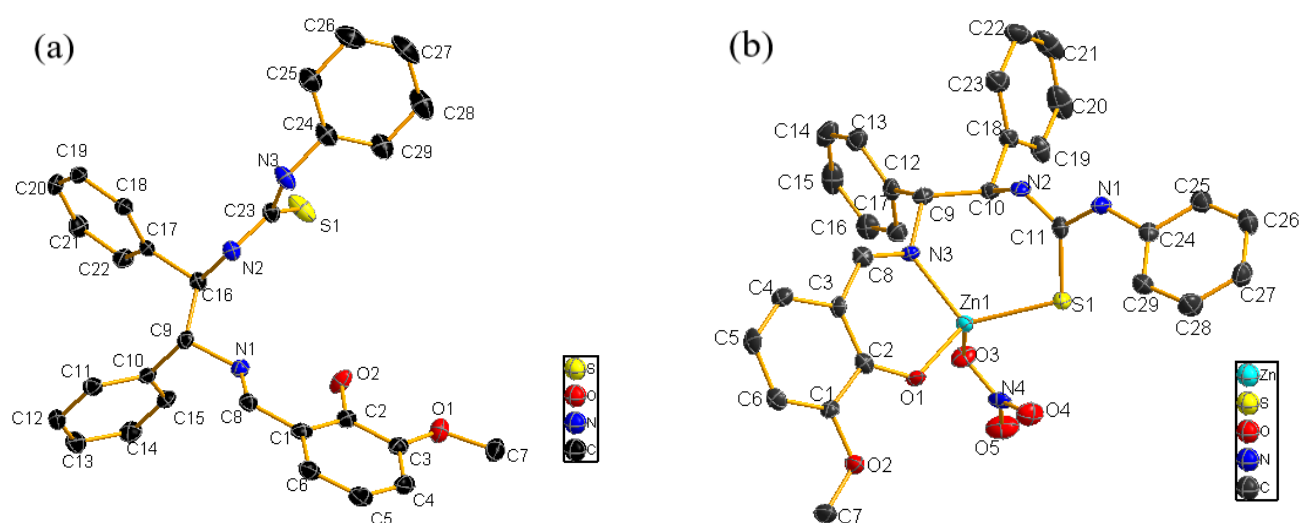


Figure 5. Oka Ridge Thermal Ellipsoidal plot (ORTEP) diagrams of **HL**₄ (a) and **L**₄- ZnNO_3 (b) with the atom numbering schemes at the 40% probability level. Hydrogen atoms and solvent molecules are omitted for clarity.

Coordination mechanism studies confirm that **HL** and $\text{Zn}(\text{NO}_3)_2$ form strongly fluorescent complexes, which suggests 1:1 binding stoichiometry between **HL** and $\text{Zn}(\text{NO}_3)_2$. Through the single-crystal structure of the complex, it can be visually seen that the atoms coordinated with Zn^{2+} include O atoms provided by phenolic hydroxyl groups, N atoms provided by Schiff bases, and S atoms provided by thiourea structural units. Zn^{2+} with **HL** forms a six-membered ring and a seven-membered ring with coordination atoms.

2.3. Theoretical Study

Density Functional Theory (DFT) calculations and time-dependent DFT (TD-DFT) using B3LYP were carried out with Gaussian 09 software package ADDIN EN.CITE [37]. The 6-31G(d,p) basis set was employed for C, H, N, O, and S atoms, and the LANL2DZ basis set was employed for the Zn atom [38,39]. Full geometry optimizations of the **HL**₄ and **L**₄-**ZnNO**₃ in the singlet ground-state were carried out using the DFT method (Figure 6). The assignment of the type of each MO is made on the basis of its composition. The frontier molecular orbital results from the extension geometries show that the spatial distributions of the HOMO (HOMO = highest occupied molecular orbital) and LUMO (LUMO = lowest unoccupied molecular orbital) are both localized with the phenol moiety with a bandgap of 4.243 eV. However, after the complexation of **HL**₄ with Zn^{2+} , the HOMOs of **L**₄-**ZnNO**₃ were spread over the phenol moiety, and the LUMOs extended to the Zn^{2+} and thiourea moiety with the bandgap of 3.732 eV, which indicates the possible electron transfer from ligand to metal (LMCT). The theoretical bond length between S and O was 5.12262 Å before adding Zn^{2+} , and was shortened to 4.05971 Å after forming a complex with **HL**₄, which was consistent with the change in the crystal data.

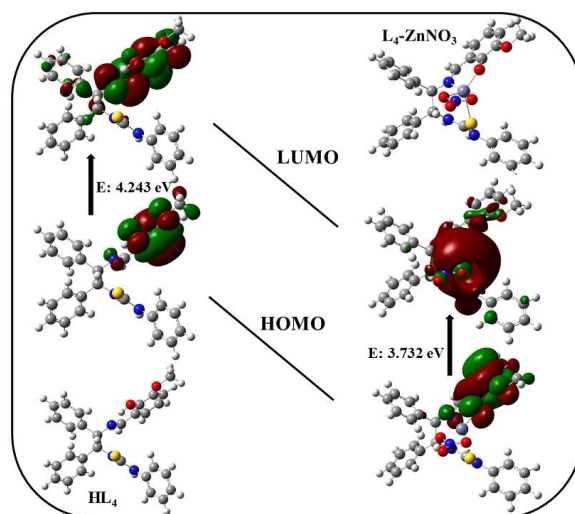


Figure 6. Frontier molecular orbitals of probe **HL**₄ and **L**₄-**ZnNO**₃ as obtained from DFT calculations.

2.4. Fluorescence Studies of **L**-**ZnNO**₃ in the Presence of Anions

2.4.1. Anion Selectivity Experiments

Different zinc salt selectivity experiments revealed that different kinds of anions could affect the Zn^{2+} recognition performance. To investigate the effect of different kinds of anions on zinc complexes, anion selectivity experiments were performed. When excited at 377 nm, **L**₁-**ZnNO**₃ displayed a strong emission peak at 449 nm. Among a set of different anions (Cl^- , Br^- , F^- , CH_3COO^- , NO_3^- , $\text{C}_6\text{H}_5\text{COO}^-$, $\text{C}_6\text{H}_5\text{SO}_2^-$, PO_4^{2-} , H_2PO_4^- , HPO_4^{2-} , SO_3^{2-} , SO_4^{2-} , H_2PO_2^- , NO_2^- , NO_3^- , and SCN^-), a prominent change in the emission spectra of **L**₁-**ZnNO**₃ manifested upon the addition of H_2PO_4^- alone (Figure 7). When **L**₁-**ZnNO**₃ was combined with H_2PO_4^- , the bright blue color of the solution disappeared, resulting in a colorless transparent solution (Figure 7, insert and Figure S5). A similar phenomenon also occurred when adding H_2PO_4^- to **L**₂-**ZnNO**₃, **L**₃-**ZnNO**₃, **L**₄-**ZnNO**₃, **L**₅-**ZnNO**₃, and **L**₆-**ZnNO**₃ (Figure S6). The above experimental results proved that this

type of fluorescent probe could realize the “turn-on–turn-off” behavior, thus realizing the recognition function of cation and anion.

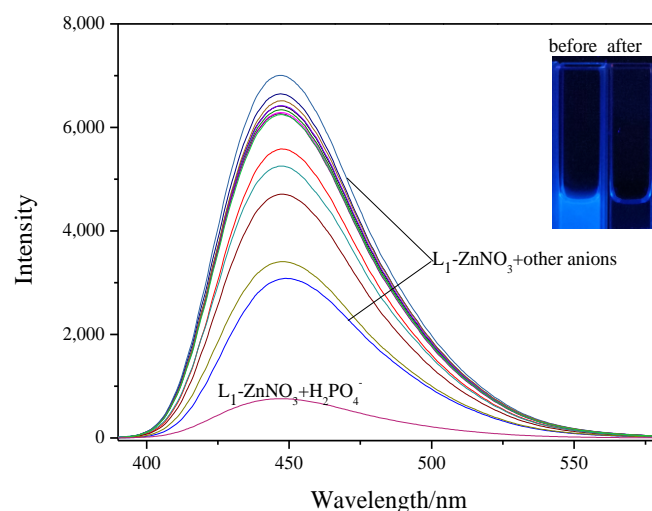


Figure 7. Fluorescence spectra of $L_1\text{-Zn}^{2+}\text{-NO}_3^-$ in acetonitrile with different anions dissolved in filtered Milli-Q water.

2.4.2. Anion-Competitive Experiments

To verify the influence of other anions on the probe recognition of H_2PO_4^- , the emission intensity of the probe and H_2PO_4^- at 450 nm ($\lambda_{\text{ex}} = 370$ nm) was monitored (Figure 8a). The result showed that the $L_1\text{-ZnNO}_3$ could specifically detect H_2PO_4^- in the presence of other related anions. The anion-competitive experiments of $L_2\text{-ZnNO}_3$, $L_3\text{-ZnNO}_3$, $L_4\text{-ZnNO}_3$, $L_5\text{-ZnNO}_3$, and $L_6\text{-ZnNO}_3$ are shown in the Supplementary Materials (Figure S7), which were generally consistent with $L_1\text{-ZnNO}_3$.

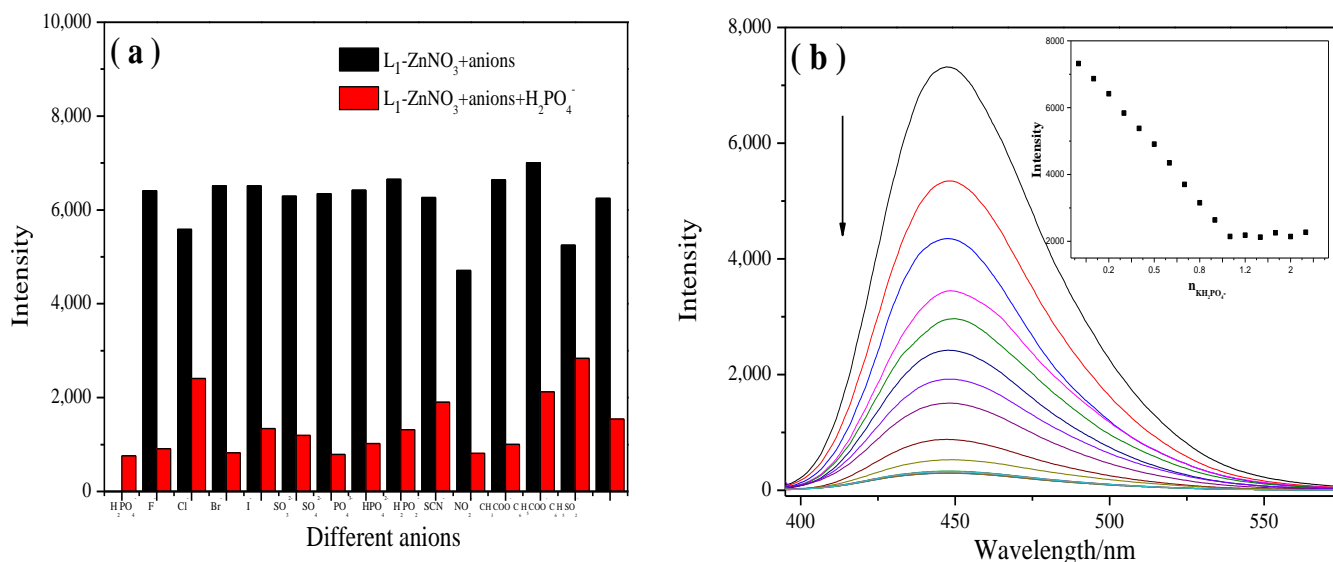


Figure 8. (a) Comparison of fluorescence intensity before and after the addition of $L_1\text{-ZnNO}_3$ in acetonitrile; (b) fluorescence emission spectra of $L_1\text{-ZnNO}_3$ in acetonitrile solution with the addition of H_2PO_4^- . Inset: Fluorescence intensity of $L_1\text{-ZnNO}_3$ depending on the H_2PO_4^- in the range from 0 to 2.0 equiv.

The titration of $L_1\text{-ZnNO}_3$ with H_2PO_4^- triggered a distinct decrease in the emission intensity at 450 nm (Figure 8b). $L_2\text{-ZnNO}_3\sim L_6\text{-ZnNO}_3$ and H_2PO_4^- are exhibited in the Supplementary Materials (Figure S8).

In this work, a series of novel chiral thiourea fluorescent probes **HL**₁–**HL**₆ were prepared for the first time for fluorescence-responsive Zn²⁺, while their complex **L-Zn-NO**₃ was continuously identified and detected the phosphate anion (H₂PO₄[−]). Compared with other working probes for the detection of analytes (Table S4) [7,40–46], the probes synthesized in this work have the advantages of high sensitivity and low detection limits.

3. Materials and Methods

3.1. General Procedures

3.1.1. Reagents and Instruments

All of the materials used for synthesis were purchased from commercial suppliers and used as received. Nitrate salts of Ag⁺, Na⁺, K⁺, Co²⁺, Fe³⁺, Cu²⁺, Cd²⁺, Cr³⁺, Mg²⁺, Pb²⁺, Ni²⁺, and Zn²⁺, sulfate salts of Fe²⁺ and Hg²⁺, and chlorine salt of Ca²⁺ were used for the spectroscopic studies. The different sodium salts of F[−], Cl[−], Br[−], CH₃COO[−], C₆H₅COO[−], C₆H₅SO₂[−], PO₄^{3−}, H₂PO₄[−], HPO₄^{2−}, SO₃^{2−}, SO₄^{2−}, H₂PO₂[−], NO₂[−], NO₃[−], and SCN[−] were used for investigating anion effects. All salts were dissolved in filtered Milli-Q water to prepare aqueous ion solutions.

The melting points of the products were determined on an X-4 binocular microscope. ¹H and ¹³C NMR spectra were recorded on a Bruker 400 MHz instrument at room temperature. Chemical shifts were measured relative to residual solvent peaks of CDCl₃ (¹H: δ = 7.26 ppm; ¹³C: δ = 77.0 ppm) or DMSO-*d*₆ (¹H: δ = 2.50 ppm; ¹³C: δ = 39.5 ppm) with tetramethylsilane (TMS) as internal standard. The following abbreviations are used to describe spin multiplicities in ¹H NMR spectra: s = singlet; d = doublet; t = triplet; m = multiplet. Specific rotations were measured on a PerkinElmer 341 MC polarimeter. HRMS data were obtained using a 7.0T FT-ICR MS spectrometer. X-ray crystal diffraction measurements of **L** were acquired using a Bruker SMART APEX II CCD diffractometer. Fluorescence spectra were examined on a Hitachi FL-2700 spectrophotometer using 10 mm path length quartz cuvettes at 298 K. The pH was calculated by STARTER 3100/F.

3.1.2. Synthesis of **HL**₁–**HL**₆ and Compound **3**

The synthetic route for **HL**₁–**HL**₆ and compound **3** is shown in Figure 1. Under ice-cold conditions, (1*R*,2*R*)-1,2-diphenylethylenediamine (**1**, 4.71 mmol) was dissolved in dichloromethane under ice-cold conditions with constant stirring. Isothiocyanate (4.71 mmol) was dissolved in dichloromethane and then added dropwise to the above amine system via a constant pressure dropping funnel. The reaction mixture was stirred for 12 h and then evaporated under low pressure. The crude product was purified by silica gel column chromatography using dichloromethane as an eluent to give the chiral primary amine thiourea **2** in the form of a white powder. Compound **2** and the substituted aldehydes were dissolved in an ethanol solvent and heated to reflux under nitrogen protection for 24 h. The mixture was cooled and washed with ether (3 × 50 mL) to give the solid products **HL**₁–**HL**₆ and compound **3**.

1-((1*R*,2*R*)-2-(((*E*)-2-Hydroxybenzylidene)amino)-1,2-diphenylethyl)-3-phenylthiourea (**HL**₁). White solid, 70% yield, m.p. 104–108 °C; [α]_D²³ = +33.44 (c = 10, CH₂Cl₂); ¹H NMR (CDCl₃, 400 MHz) δ 12.54–12.23 (m, 1H), 8.06 (s, 1H), 7.69 (s, 1H), 7.48–7.28 (m, 7H), 7.24–6.74 (m, 13H), 5.99 (s, 1H), 4.81 (d, *J* = 4.1 Hz, 1H); ¹³C NMR (CDCl₃, 101 MHz) δ 180.5, 167.2, 160.6, 138.6, 138.2, 137.4, 135.7, 133.0, 132.0, 130.3, 129.3, 128.5, 128.3, 127.9, 127.6, 127.3, 127.2, 126.3, 125.4, 124.0, 118.9, 118.4, 117.0, 64.2, 37.1, 34.4, 32.7, 31.9, 30.1, 29.7, 29.4, 26.9, 22.7, 14.1, 11.4; HRMS (ESI) *m/z* calc'd for C₂₈H₂₅N₃OS [M + H]⁺: 452.1797, found 452.1790.

1-((1*R*,2*R*)-2-(((*E*)-2,3-Dihydroxybenzylidene)amino)-1,2-diphenylethyl)-3-phenylthiourea (**HL**₂). Yellow solid, 48% yield, m.p. 146–149 °C; [α]_D²³ = +36.61 (c = 10, CH₂Cl₂); ¹H NMR (DMSO-*d*₆, 400 MHz) δ 13.20 (d, *J* = 155.7 Hz, 1H), 9.88 (s, 1H), 9.12 (s, 1H), 8.75–8.36 (m, 2H), 7.59–6.54 (m, 18H), 6.11 (t, *J* = 8.3 Hz, 1H), 5.15–4.87 (m, 1H); ¹³C NMR (DMSO-*d*₆, 101 MHz) δ 180.4, 166.9, 149.1, 145.5, 140.2, 139.8, 139.4, 128.7, 128.4 (d, *J* = 10.9 Hz), 128.3,

127.8, 127.6, 127.3, 126.9, 126.7, 123.9, 122.6, 121.9, 118.8, 118.4, 118.3, 76.5, 62.8; HRMS (ESI) m/z calc'd for $C_{28}H_{25}N_3O_2S$ $[M + H]^+$: 468.1746, found 468.1749.

1-((1*R*,2*R*)-2-(((*E*)-2-Hydroxy-5-methylbenzylidene)amino)-1,2-diphenylethyl)-3-phenylthiourea (**HL**₃). White solid, 81% yield, m.p. 139–142 °C; $[\alpha]_D^{23} = +42.78$ ($c = 10$, CH_2Cl_2); ¹H NMR (DMSO-*d*₆, 400 MHz) δ 12.45 (s, 1H), 9.75 (s, 1H), 8.48–8.16 (m, 2H), 7.39–7.03 (m, 17H), 6.82 (d, $J = 8.3$ Hz, 1H), 6.14 (t, $J = 7.6$ Hz, 1H), 4.93 (d, $J = 6.5$ Hz, 1H), 2.22 (s, 3H); ¹³C NMR (DMSO-*d*₆, 101 MHz) δ 178.1, 164.0, 155.3, 138.1, 137.7, 136.8, 131.1, 129.1, 126.2, 126.0, 125.6, 125.3, 125.2, 125.2, 125.0, 124.6, 121.9, 120.6, 116.2, 114.0, 74.3, 60.5, 17.6; HRMS (ESI) m/z calc'd for $C_{29}H_{27}N_3OS$ $[M + H]^+$: 466.1953, found 466.1958.

1-((1*R*,2*R*)-2-(((*E*)-2-Hydroxy-3-methoxybenzylidene)amino)-1,2-diphenylethyl)-3-phenylthiourea (**HL**₄). Brown solid, 84% yield, m.p. 150–152 °C; $[\alpha]_D^{23} = +48.81$ ($c = 10$, CH_2Cl_2); ¹H NMR (DMSO-*d*₆, 400 MHz) δ 12.55 (s, 1H), 9.35 (s, 1H), 8.27–7.34 (m, 2H), 7.23–6.53 (m, 17H), 6.44 (d, $J = 7.9$ Hz, 1H), 5.74 (s, 1H), 4.55 (d, $J = 6.6$ Hz, 1H), 3.39 (s, 3H); ¹³C NMR (DMSO-*d*₆, 101 MHz) δ 180.4, 166.6, 150.1, 147.8, 140.2, 139.9, 139.1, 128.5, 128.3, 127.9, 127.6, 127.5, 127.4, 126.9, 124.1, 123.0, 122.8, 118.6, 118.4, 115.0, 76.3, 62.7, 55.8; HRMS (ESI) m/z calc'd for $C_{29}H_{27}N_3O_2S$ $[M + H]^+$: 482.1902, found 482.1907.

1-((1*R*,2*R*)-2-(((*E*)-5-Chloro-2-hydroxybenzylidene)amino)-1,2-diphenylethyl)-3-phenylthiourea (**HL**₅). Yellow solid, 80% yield, m.p. 158–160 °C; $[\alpha]_D^{23} = +37.11$ ($c = 10$, CH_2Cl_2); ¹H NMR (DMSO-*d*₆, 400 MHz) δ 12.58 (s, 1H), 9.73 (s, 1H), 8.30 (d, $J = 8.0$ Hz, 2H), 7.54 (s, 1H), 7.40–7.14 (m, 16H), 7.09 (d, $J = 7.2$ Hz, 1H), 6.94 (d, $J = 8.8$ Hz, 1H), 6.14 (s, 1H), 4.93 (d, $J = 6.3$ Hz, 1H); ¹³C NMR (DMSO-*d*₆, 101 MHz) δ 180.5, 164.3, 158.4, 140.2, 132.3, 129.9, 128.5, 128.3, 127.9, 127.6, 127.5, 127.4, 127.0, 123.0, 122.4, 120.3, 118.5, 76.5, 62.7; HRMS (ESI) m/z calc'd for $C_{28}H_{24}ClN_3OS$ $[M + H]^+$: 482.1407, found 486.1412.

1-((1*R*,2*R*)-2-(((*E*)-(2-Hydroxynaphthalen-1-yl)methylene)amino)-1,2-diphenylethyl)-3-phenylthiourea (**HL**₆). Yellow solid, 74% yield, m.p. 154–156 °C; $[\alpha]_D^{23} = +46.22$ ($c = 10$, CH_2Cl_2); ¹H NMR (DMSO-*d*₆, 400 MHz) δ 14.92 (s, 1H), 9.65 (s, 1H), 9.25 (s, 1H), 8.42 (s, 1H), 8.04 (s, 1H), 7.93–7.71 (m, 2H), 7.49 (s, 1H), 7.36–7.06 (m, 15H), 6.96 (d, $J = 9.2$ Hz, 2H), 6.22 (s, 1H), 5.24 (s, 1H); ¹³C NMR (DMSO-*d*₆, 101 MHz) δ 180.4, 161.3, 139.3, 138.9, 135.9, 133.1, 129.0, 128.5, 128.0, 127.9, 127.8, 127.6, 127.5, 127.2, 126.3, 122.9, 123.0, 122.2, 119.2, 107.2, 72.7; HRMS (ESI) m/z calc'd for $C_{32}H_{27}N_3OS$ $[M + H]^+$: 502.1953, found 502.1959.

1-((1*R*,2*R*)-2-(((*E*)-Benzylidene)amino)-1,2-diphenylethyl)-3-phenylthiourea (**3**). White solid, 76% yield, m.p. 175–179 °C; $[\alpha]_D^{23} = +27.33$ ($c = 10$, CH_2Cl_2); ¹H NMR (CDCl₃, 400 MHz) δ 7.99–7.76 (m, 2H), 7.73–7.27 (m, 16H), 7.26–7.02 (m, 5H), 5.92 (s, 1H), 4.60 (s, 1H); ¹³C NMR (CDCl₃, 101 MHz) δ 180.4, 162.9, 141.2, 140.5 (d, $J = 65.6$ Hz), 135.3, 131.2, 130.2, 128.5, 128.4, 128.3, 127.6, 127.4, 127.2, 126.7, 126.1, 77.3, 64.9; HRMS (ESI) m/z calc'd for $C_{28}H_{25}N_3S$ $[M + H]^+$: 436.1847, found 436.1841.

3.2. Spectroscopic Measurements

Stock solutions of various ions (0.50 mol/L) were prepared in filtered Milli-Q water. A stock solution of **HL** probe (1.0×10^{-2} mol/L) and compound **3** in acetonitrile was freshly prepared for fluorescence measurement. Fluorescence spectroscopic measurements were recorded for samples at 1 min after the addition of various analytes. All spectroscopic measurements were performed at 25 °C. For fluorescence measurements, the excitation wavelength was fixed at 380 nm ($\lambda_{ex} = 380$ nm) and 357 nm for **HL**₁ and **HL**₂, and at 390 nm ($\lambda_{ex} = 390$ nm) for **HL**₃–**HL**₆ and compound **3**, respectively. The emission wavelength was recorded from 220 to 600 nm for **HL**₁–**HL**₆ and compound **3**. In the cation selectivity experiments, the test samples were prepared by interacting 20 μ L of the cation stock (0.50 mol/L) with 1 mL of **HL** solution (1.0×10^{-4} mol/L) and compound **3**. In the presence of other metal ions, the competition between Zn^{2+} and other metal ions was systematically studied by fluorescence emission spectroscopy. In the titration experiments, the solution of **HL** (1.0×10^{-5} mol/L) was placed in a quartz cuvette, and a certain volume

of the metal ion stock solution (5.0×10^{-4} mol/L) was added gradually to achieve a concentration of 1.0×10^{-5} mol/L. Similarly, anion experiments were conducted based on L-ZnNO₃ to study the fluorescence spectra after combination with different anions.

3.3. Synthesis of the Sensor Zn(II) Complex and X-ray Crystallography

A methanol solution (2 mL) of Zn(NO₃)₂·6H₂O (0.0297 g, 1 equiv.) was added into the round bottom flask containing acetonitrile (3 mL) and compound HL₄ (0.0482 g, 0.1 mmol). Then, it was sealed with unsintered polytetrafluoroethylene (PTFE) tapes and holes were pricked in the tape with a needle. The crystals of L₄-ZnNO₃ were obtained after the solvent slowly evaporated at room temperature.

The crystal structures were determined using a Bruker SMART APEX II CCD diffractometer with a monochromator and Cu K α radiation ($\lambda = 0.71073$ Å) at 114(2) or 146.4(3) K with an increasing ω (width of 0.3° per frame) at a scan speed of 5 s per frame. Using Olex2 [47], the structure was solved with the ShelXT [48] structure solution program using Direct Methods and refined with the ShelXL [49] refinement package using least squares minimization. All non-hydrogen atoms were refined anisotropically and the hydrogen atoms attached to all carbon atoms were geometrically fixed. The positional and temperature factors were refined isotropically.

4. Conclusions

Chiral thiourea Schiff base compounds were synthesized and their binding properties with cations were studied. The spectral data showed that the HL₁–HL₆ probes have high selectivity and sensitivity to Zn²⁺ and are not affected by the presence of other coexisting metal ions. Combined with the crystal data, it was determined that the HL and Zn(NO₃)₂ form a L-ZnNO₃ complex in a 1:1 ratio. The formed L-ZnNO₃ complex can selectively recognize H₂PO₄[−] without interference from other anions. The probe has good prospects for application and provides a new approach for the detection of Zn(NO₃)₂ and H₂PO₄[−] in actual samples.

Supplementary Materials: The following supporting information can be downloaded at <https://www.mdpi.com/article/10.3390/molecules28104166/s1>: Section S1: Fluorescence spectra and photos of L with metal ion (Figures S1–S4); Section S2: Fluorescence spectra and photos of L-ZnNO₃ with anion (Figures S5–S8); Section S3: Crystallographic data (Tables S1–S3); Section S4: Examples for detection of Zn²⁺ and phosphate anions by sensors (Table S4); Section S5: ¹H NMR and ¹³C NMR spectra of HL₁–HL₆ and **3** (Figures S9–S22).

Author Contributions: Project administration, supervision, Z.W.; chemical methodology, S.Y.; formal analysis, S.Y. and Y.H.; writing—original draft, S.Y.; writing—review and editing, H.L. and A.L. All authors have read and agreed to the published version of the manuscript.

Funding: This research was funded by the S&T Program of Hebei (21326504D) and the Natural Science Foundation of Hebei Province (B2020202028).

Institutional Review Board Statement: Not applicable.

Informed Consent Statement: Not applicable.

Data Availability Statement: All data used to support the findings of this study are included within the article and Supplementary Materials.

Acknowledgments: The authors also acknowledge the State Key Laboratory of Elemento-Organic Chemistry (Nankai University) for the characterization of the target compounds.

Conflicts of Interest: The authors declare no conflict of interest.

Sample Availability: Samples of the compounds HL₁–HL₆ and **3** are available from the authors.

References

1. Chowdhury, S.; Roj, B.; Dutta, A.; Mandal, U. Review on recent advances in metal ions sensing using different fluorescent probes. *J. Fluoresc.* **2018**, *28*, 999–1021. [[CrossRef](#)] [[PubMed](#)]
2. Hou, L.J.; Feng, J.; Wang, Y.B.; Dong, C.; Shuang, S.M.; Wang, Y. Single fluorescein-based probe for selective colorimetric and fluorometric dual sensing of Al³⁺ and Cu²⁺. *Sens. Actuators B Chem.* **2017**, *247*, 451–460. [[CrossRef](#)]
3. Zhan, Y.C.; Tsai, J.J.; Chen, Y.C. Zinc ion-based switch-on fluorescence-sensing probes for the detection of tetracycline. *Molecules* **2022**, *27*, 8403. [[CrossRef](#)] [[PubMed](#)]
4. Asiri, A.M.; Al-Ghamdi, N.S.M.; Dzudzevic-Cancar, H.; Kumar, P.; Khan, S.A. Physicochemical and Photophysical investigation of newly synthesized carbazole containing pyrazoline-benzothiazole as fluorescent chemosensor for the detection of Cu²⁺, Fe³⁺ & Fe²⁺ metal ion. *J. Mol. Struct.* **2019**, *1195*, 670–680. [[CrossRef](#)]
5. Shi, W.; Chen, Y.B.; Chen, X.; Xie, Z.F.; Hui, Y.H. Simple-structured, hydrazinecarbothioamide derivatived dual-channel optical probe for Hg²⁺ and Ag⁺. *J. Lumin.* **2016**, *174*, 56–62. [[CrossRef](#)]
6. Gale, P.A.; Caltagirone, C. Fluorescent and colorimetric sensors for anionic species. *Coord. Chem. Rev.* **2018**, *354*, 2–27. [[CrossRef](#)]
7. Banerjee, M.; Ta, S.; Ghosh, M.; Ghosh, A.; Das, D. Sequential fluorescence recognition of molybdenum(VI), arsenite, and phosphate ions in a ratiometric manner: A facile approach for discrimination of AsO₂[−] and H₂PO₄[−]. *ACS Omega* **2019**, *4*, 10877–10890. [[CrossRef](#)]
8. Wagh, Y.B.; Tayade, K.C.; Kuwar, A.; Sahoo, S.K.; Mayank; Singh, N.; Dalal, D.S. Exploration of highly selective fluorogenic “on-off” chemosensor for H₂PO₄[−] ions: ICT-based sensing and ATPase activity profiling. *Luminescence* **2020**, *35*, 379–384. [[CrossRef](#)]
9. Lu, W.; Zhang, M.Y.; Liu, K.Y.; Fan, B.; Xia, Z.; Jiang, L.M. A fluoride-selective colorimetric and fluorescent chemosensor and its use for the design of molecular-scale logic devices. *Sens. Actuators B Chem.* **2011**, *160*, 1005–1010. [[CrossRef](#)]
10. Hagimori, M.; Hara, F.; Mizuyama, N.; Fujino, T.; Saji, H.; Mukai, T. High-affinity ratiometric fluorescence probe based on 6-amino-2,2′-bipyridine scaffold for endogenous Zn²⁺ and its application to living cells. *Molecules* **2022**, *27*, 1287. [[CrossRef](#)]
11. Roy, A.; Shee, U.; Mukherjee, A.; Mandal, S.K.; Roy, P. Rhodamine-based dual chemosensor for Al³⁺ and Zn²⁺ ions with distinctly separated excitation and emission wavelengths. *ACS Omega* **2019**, *4*, 6864–6875. [[CrossRef](#)]
12. Liu, D.D.; Zhang, M.Z.; Du, W.; Hu, L.; Li, F.; Tian, X.H.; Wang, A.D.; Zhang, Q.; Zhang, Z.P.; Wu, J.Y. A series of Zn(II) terpyridine-based nitrate complexes as two-photon fluorescent probe for identifying apoptotic and living cells via subcellular immigration. *Inorg. Chem.* **2018**, *57*, 7676–7683. [[CrossRef](#)] [[PubMed](#)]
13. Winnett, M.R.; Mini, P.; Grace, M.R.; Tuck, K.L. Time-resolved terbium-based probe for the detection of zinc(II) ions: Investigation of the formation of a luminescent ternary complex. *Inorg. Chem.* **2020**, *59*, 118–127. [[CrossRef](#)]
14. Bourassa, D.; Elitt, C.M.; McCallum, A.M.; Sumalekshmy, S.; McRae, R.L.; Morgan, M.T.; Sigel, N.; Perry, J.W.; Rosenberg, P.A.; Fahrni, C.J. Chromis-1, a ratiometric fluorescent probe optimized for two-photon microscopy reveals dynamic changes in labile Zn(II) in differentiating oligodendrocytes. *ACS Sens.* **2018**, *3*, 458–467. [[CrossRef](#)]
15. Cho, J.; Verwilt, P.; Kang, M.J.; Pan, J.L.; Sharma, A.; Hong, C.S.; Kim, J.S.; Kim, S. Crown ether-appended calix[2]triazolium[2]arene as a macrocyclic receptor for the recognition of the H₂PO₄[−] anion. *Chem. Commun.* **2020**, *56*, 1038–1041. [[CrossRef](#)] [[PubMed](#)]
16. Asthana, S.K.; Pandey, A.; Kumar, A.; Upadhyay, K.K. An incisive optical recognition of monohydrogen phosphate by a fluorescein-based chemodosimeter. *New J. Chem.* **2020**, *44*, 2201–2205. [[CrossRef](#)]
17. Yao, H.; Zhou, Q.; Wang, J.; Chen, Y.Y.; Kan, X.T.; Wei, T.B.; Zhang, Y.M.; Lin, Q. Highly selective Fe³⁺ and F[−]/H₂PO₄[−] sensor based on a water-soluble cationic pillar[5]arene with aggregation-induced emission characteristic. *Spectrochim. Acta Part A Mol. Biomol. Spectrosc.* **2019**, *221*, 117215–117220. [[CrossRef](#)]
18. Zhang, D.W.; Cochrane, J.R.; Martinez, A.; Gao, G.H. Recent advances in H₂PO₄[−] fluorescent sensors. *RSC Adv.* **2014**, *4*, 29735–29749. [[CrossRef](#)]
19. Gray, R.W.; Wilz, D.R.; Caldas, A.E.; Jacob Lemann, J.R. The importance of phosphate in regulating plasma 1,25-(OH)₂-vitamin D levels in humans: Studies in healthy subjects, in calcium-stone formers and in patients with primary hyperparathyroidism. *J. Clin. Endocrinol. Metab.* **1976**, *45*, 299–306. [[CrossRef](#)]
20. Shi, B.B.; Zhang, Y.M.; Wei, T.B.; Lin, Q.; Yao, H.; Zhang, P.; You, X.M. A fluorescent and colorimetric chemosensor for dihydrogen phosphate ions based on 2-pyridine-1H-imidazo[4,5-b]phenazine–zinc ensemble. *Sens. Actuators B Chem.* **2014**, *190*, 555–561. [[CrossRef](#)]
21. Liu, F.F.; Fan, C.B.; Pu, S.Z. A new “turn-on” fluorescent chemosensor for Zn²⁺ based on a diarylethene derivative and its practical applications. *J. Photochem. Photobiol. A Chem.* **2019**, *371*, 248–254. [[CrossRef](#)]
22. Kumar, S.S.; Kumar, R.S.; Kumar, S.A. An “Off-On-Off” type fluorescent chemosensor for the relay detection of Zn²⁺ and H₂PO₄[−] in aqueous environment. *Inorg. Chim. Acta* **2020**, *502*, 119348. [[CrossRef](#)]
23. Wang, S.; Ma, L.L.; Liu, G.; Pu, S.Z. Diarylethene-based fluorescent and colorimetric chemosensor for the selective detection of Al³⁺ and CN[−]. *Dyes Pigments* **2019**, *164*, 257–266. [[CrossRef](#)]
24. Liu, Y.; Wang, X.; Feng, E.T.; Fan, C.B.; Pu, S.Z. A highly selective sequential recognition probe for Zn²⁺ and HSO₄[−]/H₂PO₄[−] based on a diarylethene chemosensor. *Spectrochim. Acta A* **2021**, *246*, 119052. [[CrossRef](#)] [[PubMed](#)]
25. Arabahmadi, R. Antipyrine-based Schiff base as fluorogenic chemosensor for recognition of Zn²⁺, Cu²⁺ and H₂PO₄[−] in aqueous media by comparator, half subtractor and integrated logic circuits. *J. Photochem. Photobiol. A Chem.* **2022**, *426*, 113762. [[CrossRef](#)]

26. Liu, G.; Zhao, L. A simple colorimetric and on-off fluorescent chemosensor for biologically important anions based on thiourea groups. *Spectrosc. Lett.* **2012**, *45*, 424–429. [CrossRef]
27. Chowdhury, B.; Sinha, S.; Ghosh, P. Substitution effect on near infrared absorbance based selective fluoride sensing of indole functionalized thiourea molecules. *Eur. J. Org. Chem.* **2019**, *5*, 1008–1015. [CrossRef]
28. Sinha, S.; Dey, G.; Kumar, S.; Mathew, J.; Mukherjee, T.; Mukherjee, S.; Ghosh, S. Cysteamine-based cell-permeable Zn²⁺-specific molecular bioimaging materials: From animal to plant cells. *ACS Appl. Mater. Interfaces* **2013**, *5*, 11730–11740. [CrossRef]
29. Powell, K.J.; Brown, P.L.; Byrne, R.H.; Gajda, T.; Hefter, G.; Leuz, A.-K.; Sjöberg, S.; Wanner, H. Chemical speciation of environmentally significant metals with inorganic ligands. Part 5: The Zn²⁺ + OH[−], Cl[−], CO₃^{2−}, SO₄^{2−}, and PO₄^{3−} systems (IUPAC Technical Report). *Pure Appl. Chem.* **2013**, *85*, 2249–2311. [CrossRef]
30. Hibberta, D.B.; Thordarson, P. The death of the Job plot, transparency, open science and online tools, uncertainty estimation methods and other developments in supramolecular chemistry data analysis. *Chem. Commun.* **2016**, *52*, 12792–12805. [CrossRef]
31. Available online: <http://supramolecular.org> (accessed on 9 May 2016).
32. Thordarson, P. Determining association constants from titration experiments in supramolecular chemistry. *Chem. Soc. Rev.* **2011**, *40*, 1305–1323. [CrossRef] [PubMed]
33. Datta, B.K.; Thiyagarajan, D.; Ramesh, A.; Das, G. A sole multi-analyte receptor responds with three distinct fluorescence signals: Traffic signal like sensing of Al³⁺, Zn²⁺ and F[−]. *Dalton Trans.* **2015**, *44*, 13093–13099. [CrossRef]
34. Valencia, L.; Pérez-Lourido, P.; Bastida, R.; Macias, A. Dinuclear Zn(II) polymer consisting of channels formed by π,π -stacking interactions with a flow of nitrate anions through the channels. *Cryst. Growth Des.* **2008**, *8*, 2080–2082. [CrossRef]
35. Dolai, M.; Mistri, T.; Panja, A.; Ali, M. Diversity in supramolecular self-assembly through hydrogen-bonding interactions of non-coordinated aliphatic –OH group in a series of heterodinuclear CuII/M (M=NaI, ZnII, HgII, SmIII, BiIII, PbII and CdII). *Inorg. Chim. Acta* **2013**, *399*, 95–104. [CrossRef]
36. Zhu, Y.; Xia, C.K.; Meng, S.C.; Chen, J.; Chen, J.; Xie, J.M. Syntheses, structures, properties and DFT calculations of coordination polymers constructed by 2,6-bis(benzimidazolyl)pyridine. *Polyhedron* **2013**, *61*, 181–187. [CrossRef]
37. Frisch, M.J.; Trucks, G.W.; Schlegel, H.B.; Scuseria, G.E.; Robb, M.A.; Cheeseman, J.R.; Montgomery, J.A.; Vreven, T.; Kudin, K.N.; Burant, J.C.; et al. *Revision A.01*; Gaussian, Inc.: Wallingford, CT, USA, 2009.
38. Lee, C.; Yang, W.; Parr, R.G. Development of the Colle-Salvetti correlation-energy formula into a functional of the electron density. *Phys. Rev. B* **1988**, *37*, 785–789. [CrossRef]
39. Miehlich, B.; Savin, A.; Stoll, H.; Preuss, H. Results obtained with the correlation energy density functionals of Becke and Lee, Yang and Parr. *Chem. Phys. Lett.* **1989**, *157*, 200–206. [CrossRef]
40. Paulpandi, R.Q.; Ramasamy, S.; Paulraj, M.S.; Baños, F.G.D.; Villora, G.; Cerón-Carrasco, J.P.; Pérez-Sánchez, H.; Enoch, I.V.M.V. Enhanced Zn²⁺ ion-sensing behavior of a benzothiazole derivative on encapsulation by β -cyclodextrin. *RSC Adv.* **2016**, *6*, 15670–15677. [CrossRef]
41. Dong, Z.; Le, X.; Zhou, P.; Dong, C.; Ma, J. An “off-on-off” fluorescent probe for the sequential detection of Zn²⁺ and hydrogen sulfide in aqueous solution. *New J. Chem.* **2014**, *38*, 1802–1808. [CrossRef]
42. Dong, Z.; Le, X.; Zhou, P.; Dong, C.; Ma, J. Sequential recognition of zinc ion and hydrogen sulfide by a new quinoline derivative with logic gate behavior. *RSC Adv.* **2014**, *4*, 18270–18277. [CrossRef]
43. Shyamal, M.; Mazumdar, P.; Maity, S.; Samanta, S.; Sahoo, G.P.; Misra, A. Highly selective turn-on fluorogenic chemosensor for robust quantification of Zn(II) based on aggregation induced emission enhancement feature. *ACS Sens.* **2016**, *1*, 739–747. [CrossRef]
44. He, X.; Xie, Q.; Fan, J.; Xu, C.; Xu, W.; Li, Y.; Ding, F.; Deng, H.; Chen, H.; Shen, J. Dual-functional chemosensor with colorimetric/ratiometric response to Cu(II)/Zn(II) ions and its applications in bioimaging and molecular logic gates. *Dyes Pigments* **2020**, *177*, 108255. [CrossRef]
45. Moradi, S.; Molavipordanjani, S.; Hosseinimehr, S.J.; Emami, S. Benzo[d]imidazo[2,1-b]thiazole-based fluorescent sensor for Zn²⁺ ion detection. *J. Photochem. Photobiol. A* **2020**, *389*, 112184. [CrossRef]
46. Sethupathi, M.; Jayamani, A.; Muthusankar, G.; Sakthivel, P.; Sekar, K.; Gandhid, S.; Sengottuvelan, N.; Gopu, G.; Selvaraju, C. Colorimetric and fluorescence sensing of Zn²⁺ ion and its bio-imaging applications based on macrocyclic “tet a” derivative. *J. Photochem. Photobiol. B* **2020**, *207*, 11854. [CrossRef] [PubMed]
47. Dolomanov, O.V.; Bourhis, L.J.; Gildea, R.J.; Howard, J.A.K.; Puschmann, H. OLEX2: A complete structure solution, refinement and analysis program. *J. Appl. Crystallogr.* **2009**, *42*, 339–341. [CrossRef]
48. Sheldrick, G.M. SHELXT-Integrated space-group and crystal-structure determination. *Acta Crystallogr. A-Found. Adv.* **2015**, *A71*, 3–8. [CrossRef]
49. Sheldrick, G.M. Crystal structure refinement with SHELXL. *Acta Crystallogr. C Struct. Chem.* **2015**, *C71*, 3–8. [CrossRef]

Disclaimer/Publisher’s Note: The statements, opinions and data contained in all publications are solely those of the individual author(s) and contributor(s) and not of MDPI and/or the editor(s). MDPI and/or the editor(s) disclaim responsibility for any injury to people or property resulting from any ideas, methods, instructions or products referred to in the content.